Reprint Series
11 October 1996, Volume 274, pp. 236–238

SCIENCE

Femtosecond X-ray Pulses at 0.4 Å Generated by 90° Thomson Scattering: A Tool for Probing the Structural Dynamics of Materials

R. W. Schoenlein,* W. P. Leemans, A. H. Chin, P. Volfbeyn,
T. E. Glover, P. Balling, M. Zolotorev, K.-J. Kim,
S. Chattopadhyay, and C. V. Shank

Femtosecond X-ray Pulses at 0.4 Å Generated by 90° Thomson Scattering: A Tool for Probing the Structural Dynamics of Materials

R. W. Schoenlein,* W. P. Leemans, A. H. Chin, P. Volfbeyn, T. E. Glover, P. Balling, M. Zolotorev, K.-J. Kim, S. Chattopadhyay, C. V. Shank

Pulses of x-rays 300 femtoseconds in duration at a wavelength of 0.4 angstroms (30,000 electron volts) have been generated by 90° Thomson scattering between infrared terawatt laser pulses and highly relativistic electrons from an accelerator. In the right-angle scattering geometry, the duration of the x-ray burst is determined by the transit time of the laser pulse across the ~90-micrometer waist of the focused electron beam. The x-rays are highly directed (~0.6° divergence) and can be tuned in energy. This source of femtosecond x-rays will make it possible to combine x-ray techniques with ultrafast time resolution to investigate structural dynamics in condensed matter.

Understanding the structural dynamics of materials on the fundamental time scale for atomic motion represents an important frontier in condensed matter research because chemical reactions, phase transitions, and surface processes are ultimately driven by the motion of atoms on the time scale of one vibrational period (~100 fs). To date, the study of ultrafast structural dynamics in the fields of physics, chemistry, and biology has relied largely on femtosecond optical pulses generated from mode-locked lasers (*1*). However, optical radiation is restricted to the probing of extended electronic levels in solids, which are poor indicators of atomic structure. X-rays interact with core electronic levels and are therefore effective structural probes; but existing synchrotron sources of high-brightness x-rays are two orders of magnitude too slow to resolve atomic motion on the 100-fs time scale. In this report we describe the generation of a directed beam of femtosecond x-rays by the scattering of a terawatt laser pulse off relativistic electrons. The application of such ultrashort x-ray pulses with techniques such as x-ray diffraction and extended x-ray absorption fine structure (EXAFS) will allow direct observation of structural dynamics on a femtosecond time scale.

The generation of high-energy photons by scattering between laser light and relativistic electrons was originally proposed more than three decades ago (*2*, *3*). Most recently, experimental observations of high-energy photons generated by scattering between counterpropagating electrons and long laser pulses have been reported (*4*–*6*). Similar backscattering configurations have also been proposed as a basis for free-electron lasers and synchrotron x-ray sources (*7*, *8*). However, in a backscattering geometry, the duration of the scattered x-ray burst is determined by the length of the electron bunch. Typical electron-bunch durations of several picoseconds or longer present a significant limitation for generating x-ray pulses of a duration that is relevant for fundamental studies of structural dynamics in materials.

In this report we show experimentally that femtosecond x-rays can be generated by means of a 90° Thomson scattering geometry (*9*). By crossing the photon and electron beams at a right angle, we were able to limit the interaction interval to the transit time of the laser pulse across the waist of the electron beam. Ultrashort interaction times are achieved when the electron beam is tightly focused (*10*) to ~90 μm in diameter, which results in durations for the scattered x-ray pulse of ~300 fs. Tighter focusing of the electron beam holds the potential for generating even shorter x-ray pulses, on the order of 50 fs or less (*11*). Thomson-scattered femtosecond x-rays are emitted in a highly directed beam with a divergence on the order of $1/\gamma$ (~10 mrad in the present case), where γ is the energy of the electrons relative to the electron rest energy. In addition, the x-ray pulses are absolutely synchronized to the optical femtosecond pulses, which is critical for applying pump-probe techniques with ultrafast visible and x-ray pulses.

A schematic illustration of the 90° Thomson scattering geometry is shown in Fig. 1. The interaction between a relativistic electron and a transient electromagnetic wave can be described by either a scattering picture or an undulator model because the radiation pattern in both cases is that of a (relativistically transformed) oscillating dipole (*9*, *12*). For highly relativistic electrons in a weak undulator with a deflection parameter $K = e\mathcal{E}_0\lambda_{laser}/2\pi mc^2 \ll 1$ (where $\mathcal{E}_0$ is the peak electric field of the laser pulse, λ_{laser} is the laser wavelength, e is the electron charge, m is the electron rest mass, and c is the speed of light), the energy of the scattered x-ray photons is given by

$$E = E_{laser}2\gamma^2\frac{(1 - \cos\Psi)}{(1 + \gamma^2\theta_x^2)} \qquad (1)$$

where $E_{laser} = hc/\lambda_{laser}$ is the laser photon energy (h is Planck's constant), Ψ is the interaction angle between the electrons and photons ($\Psi = \pi/2$ in our experiments), and $\theta_x \ll 1$ is the x-ray emission angle relative to the electron trajectory ($\theta_x = \theta$ for electrons traveling along z, see Fig. 1). Thus, there is a one-to-one correspondence between θ_x and E. Relativistic effects cause the x-ray flux to be strongly peaked in the forward direction; for the 50-MeV electron beam energy ($\gamma = 98$) and the 800-nm laser wavelength used in our experiments, the Thomson-scattered x-rays are peaked at a maximum energy $E_0 = 2\gamma^2E_{laser} = 30$ keV (0.4 Å). Because the laser photon energy in the rest frame of the electron ($\gamma E_{laser} = 152$ eV) is much less than the electron rest energy, Compton recoil can be neglected.

We conducted our experiments with 50-MeV electrons from a linear accelerator (linac) (*13*) and terawatt optical pulses from a laser system (*14*) based on chirped-pulse amplification in Ti:sapphire (*15*, *16*). The electrons were brought to a tight focus in an ultrahigh-vacuum interaction chamber and were then diverted by a bend-

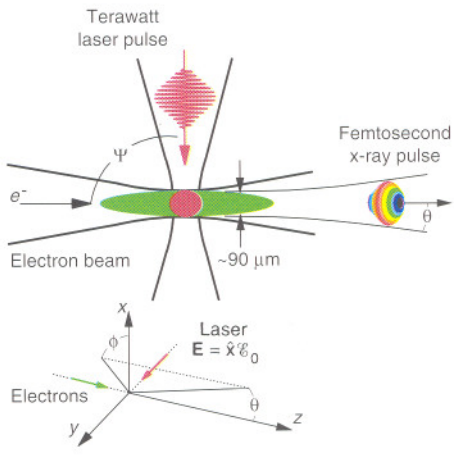

Fig. 1. Schematic of the femtosecond Thomson scattering geometry.

R. W. Schoenlein, T. E. Glover, P. Balling, Materials Sciences Division, Lawrence Berkeley National Laboratory, Berkeley, CA 94720, USA.
W. P. Leemans, P. Volfbeyn, M. Zolotorev, K.-J. Kim, S. Chattopadhyay, Accelerator and Fusion Research Division, Center for Beam Physics, Lawrence Berkeley National Laboratory, Berkeley, CA 94720, USA.
A. H. Chin, Department of Physics, University of California, Berkeley, CA 94720, USA.
C. V. Shank, Materials Sciences Division, Lawrence Berkeley National Laboratory, and Department of Physics, University of California, Berkeley, CA 94720, USA.
*To whom correspondence should be addressed.

magnet, providing direct access to the Thomson x-rays. Terawatt laser pulses (*s*-polarized, see Fig. 1) were focused by a mirror with a 75-cm radius of curvature to a spot 30 μm in diameter at the interaction point.

In this experiment, the size of the electron beam focus is critical because it determines the duration of the x-ray pulse. In addition, spatial and temporal overlap of the optical and electron pulses is crucial to ensure that Thomson x-rays are generated reliably on every shot. The spot size and position of the electron beam at the interaction point were measured by imaging optical transition radiation (OTR) from the electron beam focus onto a charge-coupled-device (CCD) camera (*17*). The laser system was synchronized with the linac by phase-locking techniques (*18*). Timing jitter was directly measured with a visible streak camera, which simultaneously detected a laser pulse and an OTR pulse from an electron bunch striking a foil. Measurements indicated a root mean square time jitter of <2 ps (*19*). An optical delay line was used to adjust the temporal overlap between the laser and electron pulses.

As a means of detecting the Thomson-scattered femtosecond x-ray beam, we used a phosphor screen, which is sensitive to x-rays in the range 10 to 50 keV. Visible photons from the phosphor were imaged onto a CCD camera to provide information about the flux, spatial profile, and position of the x-rays. We calibrated the sensitivity of the phosphor and the collection efficiency of the CCD camera and imaging system by using x-ray lines from a radioactive source (^{129}I) of known strength. Figure 2 shows an image of the x-ray beam taken from a phosphor positioned 80 cm from the interaction point. The x-rays are created by laser–electron beam scattering because they are observed only when both the laser and electron beams are present. Background radiation (bremsstrahlung x-rays) from the electron beam traveling through the beam line was subtracted. We optimized the x-ray signal and measured the spatial and temporal cross-correlation of the laser pulse with the electron bunch by recording the integrated x-ray flux as the vertical tilt of the focusing mirror or the optical delay stage were scanned. Such measurements provide detailed information about the electron bunch duration and vertical profiles of the electron and laser beams (*20*).

Integrating the total number of counts on the CCD image in Fig. 2 indicates an x-ray flux of ~5 × 10^4 photons per pulse. This flux is the total number of Thomson-scattered photons within the spectral range of the phosphor and is consistent with an estimate of the number of scattered photons ($N_{x\text{-rays}}$) based on the Thomson scattering cross section ($\sigma_T \cong 7 \times 10^{-25}$ cm^2) given by

$$N_{x\text{-rays}} \approx \frac{N_{laser} N_e}{A} \frac{\tau_{laser}}{\tau_e} \sigma_T \qquad (2)$$

where N_{laser} and N_e are, respectively, the total number of photons and electrons within the interaction area A, and τ_{laser} and τ_e are the laser and electron pulse durations, respectively ($\tau_{laser} < \tau_e$). The experimental parameters corresponding to the data of Fig. 2 are as follows: ~60-mJ, 100-fs [full width at half maximum (FWHM)] laser pulses; electron bunches of ~1.3 nC, 20 ps (FWHM); and an interaction region 90 μm in diameter. Also shown in Fig. 2 are lineouts indicating the profile of the femtosecond x-ray beam. The measured image size on the phosphor (~12 mm by ~8 mm) is consistent with the expected beam divergence $\theta \sim 1/\gamma$. The ellipticity of the image results from astigmatic focusing of the electrons, which causes a stronger electron-beam divergence (and therefore a stronger x-ray beam divergence) in the *yz* plane than in the *xz* plane. The dependence of the x-ray beam profile on the electron distribution makes it a sensitive indicator of the electron-beam properties (*20*).

The energy spectrum of the femtosecond x-rays is also strongly dependent on the electron-beam properties. The number of x-ray photons (both *s*- and *p*-polarized) per solid angle Ω scattered by a single relativistic electron in a periodic electric field of N_u cycles is given by (*12*)

$$\frac{dn}{d\Omega} = 2\alpha K^2 \gamma^2 N_u \chi^2 \left[\frac{1}{2} + \chi(\chi - 1)(\cos 2\phi_x + 1)\right] \qquad (3)$$

where α is the fine-structure constant, $\chi = E/E_0 = 1/(1 + \gamma^2\theta_x^2)$ from Eq. 1, and ϕ_x is the azimuthal angle measured relative to the electric field polarization direction. The x-ray energy spectrum generated by N_e electrons with a distribution of angular trajectories $P_e(\theta)$ (to account for the emittance of the electron beam) is then given by

$$\frac{dn}{dE d\Omega_0} = \frac{\tau_{laser}}{\tau_e} 3\alpha K^2 N_u N_e \times \frac{1}{E_0} \int_0^{2\pi} \left[\frac{1}{2} + \chi(\chi - 1)(\cos 2\phi' + 1)\right] P_e(\theta) d\phi' \qquad (4)$$

which is simply the convolution of Eq. 3 with the electron distribution expressed in a coordinate system (θ′ and θ′) that has been shifted by the detector observation angles (θ_0 and ϕ_0) so that the x-ray energy *E* is a constant of the integration path. Thus,

$$\theta^2 = \theta_0^2 + \theta'^2 - 2\theta_0\theta' \cos(\phi' - \phi_0) \qquad (5)$$

where $\theta' = \theta_x = \gamma^{-1}\sqrt{\chi - 1}$. The electron-beam divergence $P_e(\theta)$ smears the one-to-one correspondence (indicated by Eq. 1) between the observation angle θ_0 and the x-ray photon energy. X-rays propagating along a fixed θ_0 will be associated with a range of emission angles θ_x because they originate from electrons having different trajectories. As a result, the x-ray spectrum is expected to broaden to lower energies with increasing θ_0.

Figure 3 presents the results of direct measurements of the energy spectra of the

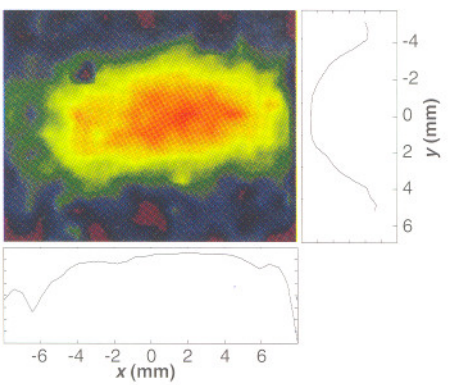

Fig. 2. False-color CCD image of the spatial profile of a 30-keV (0.4 Å), ~300-fs x-ray pulse striking a phosphor screen at a distance of 80 cm from the scattering point. Vertical and horizontal lineouts indicate a beam size of ~12 mm by ~8 mm (FWHM).

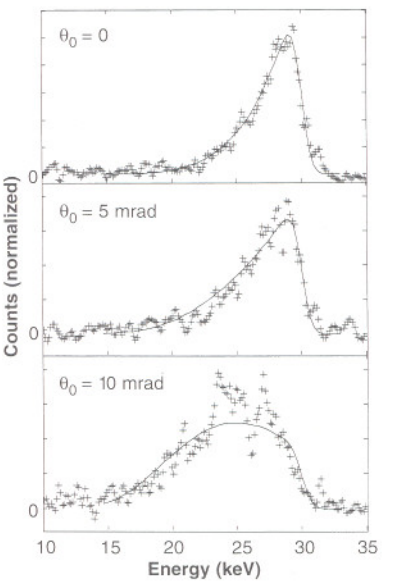

Fig. 3. Spectral measurements of the femtosecond x-rays at observation angles of θ_0 = 0 mrad, 5 mrad, and 10 mrad ($\phi_0 = \pi/2$). The detector lies in the *yz* plane. Also shown (solid lines) are theoretically predicted spectra corrected for detector sensitivity and window transmission as described in the text.

femtosecond x-rays at observation angles θ_0 = 0, 5, and 10 mrad, respectively, with $\phi_0 = \pi/2$ (the detector lies in the yz plane as defined in Fig. 1). We measured the spectra with a Ge detector (cooled with liquid nitrogen) in the photon-counting regime, using pulse-height analysis. We reduced the x-ray flux by attenuating the laser pulse, and we restricted the collection aperture of the detector to a small solid angle by using a Ta slit (100 μm by 2 mm). The on-axis spectra ($\theta_0 = 0$) were sharply peaked with a bandwidth of $\Delta E/E_0 \approx 15\%$ and a high-energy cutoff at $E_0 = 30$ keV as described by Eq. 1. At larger observation angles, the low-energy side of the spectrum broadened because of the combined effects of the electron-beam divergence and the correlation between emission angle and wavelength. In addition, there is a corresponding reduction in the measured flux.

The solid lines in Fig. 3 are theoretical predictions based on Eq. 4. The calculations include the measured experimental parameters for the laser and electron beams and have been corrected to account for the spectral sensitivity of the Ge detector, as well as the x-ray transmission characteristics of the ultrahigh-vacuum window through which the x-rays exit the interaction chamber. Because the energy spread of the electron beam is small ($\Delta\gamma/\gamma < 1\%$), its contributions to the x-ray spectrum are negligible. Contributions from the laser bandwidth (~25 nm FWHM) are included. We assume a gaussian distribution of angular trajectories for the electrons with a standard deviation of $\sigma_\theta = 3.8$ mrad (*21*), which is essentially the only free parameter in the fit aside from a uniform amplitude scaling. (The peak amplitudes of the spectra at 5 and 10 mrad are lower by factors of 0.47 and 0.06, respectively, than the peak of the 0-mrad spectrum.) The beam divergence σ_θ combined with the measured electron-beam spot size, ($\sigma_r \approx 60$ μm for the data in Fig. 3) implies an electron-beam emittance that is consistent with the measured (time-integrated) emittance, ~0.3 mm·mrad. The good agreement of the theoretical predictions with the experimental measurements indicates that the theoretical description of Thomson scattering can be used to accurately predict the characteristics of the femtosecond x-rays and their dependence on experimental conditions.

The generation of a directed beam of 300-fs x-ray pulses at 30 keV (0.4 Å) promises to be a powerful tool for studying the structural dynamics of materials on an ultrafast time scale. The x-ray pulses can be tuned by changing either the photon energy, the electron-beam energy, or the scattering angle (γ or Ψ in Eq. 1) and are absolutely synchronized to a femtosecond laser source, which is necessary for ultrafast pump-probe studies. Toward that end, we have recently measured "static" x-ray diffraction peaks from a Si ⟨111⟩ surface with the Thomson source. In this Bragg diffraction experiment, we collect ~1 diffracted x-ray photon per shot, which allows us to measure a rocking curve during only a few minutes of acquisition time. An important next step will be to apply femtosecond optical excitation and use visible–x-ray pump-probe techniques to directly observe atomic motion on an ultrafast time scale. In particular, one could directly investigate changes in long-range atomic order associated with an ultrafast solid-to-liquid phase transition by measuring the evolution of the Bragg diffraction peak on a femtosecond time scale.

The relatively low brightness of the current source (~2×10^5 photons mm^{-2} mrad^{-2} s^{-1} in a ~15% bandwidth) is best suited for diffraction studies of materials with high x-ray diffraction efficiency. The source brightness depends linearly on the average laser power and linac current; thus, successful scaling from the present 2-Hz repetition rate to 100 Hz can provide an increase in brightness of nearly two orders of magnitude. In addition, improvement of the laser pulse energy may provide another order of magnitude increase. Other factors limiting the brightness of the present source are the emittance of the electron beam (*11*) and the fact that the electron bunch is substantially longer than the x-ray pulse. Calculations based on Eq. 4 indicate that a state-of-the-art linac with a photoinjector and electron bunch compression (*22*, *23*) (providing a reduction of two orders of magnitude in electron bunch duration and a reduction of an order of magnitude in electron-beam emittance) may boost the brightness of the source by nearly three orders of magnitude. Incorporating all these factors would yield a brightness of nearly 10^{11} photons mm^{-2} mrad^{-2} s^{-1} in a ~3% bandwidth. At such levels, techniques such as EXAFS can be readily applied with femtosecond resolution to study changes in short-range order associated with chemical reactions. Rapid advances in diode-pumped, solid-state lasers and superconducting linac structures may provide substantially higher x-ray brightness in future Thomson sources by operating at very high repetition rates.

REFERENCES AND NOTES

1. P. F. Barbara, W. H. Knox, G. A. Mourou, A. H. Zewail, Eds., *Ultrafast Phenomena IX* (Springer-Verlag Series in Chemical Physics, Springer-Verlag, Berlin, 1995).
2. R. H. Milburn, *Phys. Rev. Lett.* **10**, 75 (1963).
3. F. R. Arutyunian and V. A. Tumanian, *Phys. Lett.* **4**, 176 (1963).
4. C. Bula *et al.*, *Phys. Rev. Lett.* **76**, 3116 (1996).
5. A. Ting *et al.*, *J. Appl. Phys.* **78**, 575 (1995).
6. A. M. Sandorfi *et al.*, *IEEE Trans. Nucl. Sci.* **30**, 3083 (1983).
7. J. Gea-Banacloche *et al.*, *IEEE J. Quantum Electron.* **23**, 1558 (1987).
8. P. Sprangle, A. Ting, E. Esarey, A. Fishher, *J. Appl. Phys.* **72**, 5032 (1992).
9. K.-J. Kim, S. Chattopadhyay, C. V. Shank, *Nucl. Instrum. Methods Phys. Res. A* **341**, 351 (1994).
10. Shorter x-ray pulse durations can be achieved for crossing angles Ψ less than 90°. For small crossing angles ($\Psi \ll 1$) the x-ray pulse duration scales as $\tau_{x\text{-}ray} \propto \Psi$; however, the scattering efficiency is substantially reduced, $N_{x\text{-}rays} \propto \Psi$.
11. Tighter focusing (or increased emittance) results in a larger electron-beam divergence and a broader scattered x-ray spectrum (see Eq. 4). The electron-beam size in this work represents a compromise of x-ray pulse duration, spectral bandwidth, and beam divergence.
12. A. Hofmann, in *Scottish Universities' Summer School in Physics*, C. N. Greaves and I. H. Munro, Eds. (Scottish Universities Summer School in Physics, Edinburgh, 1985), pp. 28–38.
13. We conducted the experiments at the Beam Test Facility of the Center for Beam Physics at the Berkeley Laboratory, using the linac injector for the Advanced Light Source. See W. Leemans *et al.*, in *Advanced Accelerator Concepts—AIP Conference Proceedings 335*, P. Schoessow, Ed. (American Institute of Physics, New York, 1994), p. 209.
14. The laser system consists of a Kerr lens–mode-locked oscillator operating at a 125-MHz repetition rate. Individual pulses were extracted at 10 Hz and were stretched with a grating and a telescope based on a parabolic reflector. Amplification to the 100- to 200-mJ range was achieved in an eight-pass preamplifier and a three-pass power amplifier pumped by a Q-switched Nd:yttrium-aluminum-garnet laser. Amplified pulses were compressed in vacuum with a grating pair and were delivered to the electron-beam–interaction chamber through a vacuum beam line. Amplified laser pulse durations as short as 50 fs (peak power, 2 TW) have been measured.
15. D. Strickland and G. Mourou, *Opt. Commun.* **56**, 219 (1985).
16. C. LeBlanc *et al.*, *Opt. Lett.* **18**, 140 (1993).
17. A 350-nm Al foil on a nitrocellulose membrane was placed at the electron-beam focus. OTR is created by passing the electron beam through the foil; this procedure provided an accurate indicator of the electron-beam spot size and position. See D. W. Rule, *Nucl. Instrum. Methods Phys. Res. B* **24/25**, 901 (1987).
18. A phase-locked loop dynamically controlled the cavity length of the mode-locked femtosecond laser to maintain timing synchronization with the linac. The phase-error signal was generated by the mixing of the fourth radio-frequency (rf) harmonic of the laser repetition frequency (generated from a photodiode) with the 500-MHz master rf source for the linac. See M. J. W. Rodwell, D. M. Bloom, K. J. Weingarten, *IEEE J. Quant. Electron.* **25**, 817 (1989).
19. Measurement accuracy is limited by the instrument response of the streak camera.
20. W. P. Leemans *et al.*, *Phys. Rev. Lett.*, in preparation.
21. For a gaussian distribution of electron trajectories, the integral of Eq. 4 can be expressed in terms of modified Bessel functions.
22. B. E. Carlsten and S. J. Russel, *Phys. Rev. E* **53**, R2072 (1996).
23. P. Kung, H. Lihn, H. Wiedemann, *Phys. Rev. Lett.* **73**, 967 (1994).

24. This work was supported by the Department of Energy (DOE) under contract AC03-76SF00098 and by the National Science Foundation under grant PHY-9512693. P.V. was supported under DOE contract FDDEFG-03-95ER-40936. T.E.G. was supported by a DOE Distinguished Postdoctoral Research Fellowship. The work of P.B. was supported by the Danish National Research Council. We gratefully acknowledge the support of T. Byrne and the Advanced Light Source operations crew.

29 May 1996; accepted 5 August 1996